Simulation and forecasting of ice drift as a tool for autonomous under ice operations

Tore Mo-Bjørkelund[1*], Petter Norgren[1], and Martin Ludvigsen[1,2,3]
[1]Dept. of Marine Technology, Norwegian Univ. of Sci. and Tech. (NTNU), Trondheim, Norway
[2]Center for Autonomous Marine Operations and Systems (AMOS), NTNU, Trondheim, Norway
[3]Arctic Technology Department, University Centre in Svalbard (UNIS), Longyearbyen, Norway

***Abstract*—This paper explores the use of model based ensemble forecasting and Gaussian process (GP) modelling of ice drift as a risk reducing and situational awareness tool for supporting under ice operations with autonomous underwater vehicles (AUVs). Ice tethered navigation buoys will be used to guide the vehicle under the ice and back to the ice-relative starting position. As an operational tool, we have developed a forecast model, where we attempt to predict the final destination of the vehicle, the total AUV path length, the drift of the buoys, and the properties of the underlying velocity field of drifting ice. The operation is a part of the Nansen Legacy project, and is planned for the Barents sea in May 2020. Ice and ocean in the Barents sea are in constant flux, and forecasting the motion of the ice gives insight into how the vehicle will move, and if it gets lost, where to start the search. In order to test our model, we have developed a simulator in which we can simulate the trajectories of the ice at a higher spatiotemporal resolution than most ice models. We present the simulator along with the method of forecasting where a model for each buoy is estimated and a GP is used to estimate the vector field. The divergence of the vector field is then used as an indicator of the probability of nonlinear events such as lead or pressure ridge formation. The forecast accuracy is analysed, and we can observe a dependence on spatiotemporal covariance.**

***Index Terms*—AUV, under-ice, arctic, Gaussian process, ice drift, forecast.**

I. Introduction

The challenge of under ice operations with Autonomous Underwater Vehicles (AUVs) has been present since the dawn of AUVs [1]–[3]. Pieces of expensive hardware and collected data have been lost under the polar ice sheets over the past decades [4]. In 2021, the Nansen Legacy Project will make an attempt in the northern Barents sea. The Nansen Legacy is a collaborative project between ten Norwegian research institutions with Arctic marine expertise, with a focus on the Barents sea. The operation will utilise the NTNU REMUS 100 AUV [5], and navigation buoys developed at NTNU, Trondheim and presented in [6]. The buoys will be used for both acoustic communication and navigation, and are equipped with Woods Hole Oceanographic Institution (WHOI) Micromodems [7], Global Navigation and Satellite System (GNSS) receivers and Very High Frequency (VHF) radios for inter-buoy communication as well as an Iridium module for satellite communication. The buoys will be placed along the planned transect of the vehicle in the drift ice, with one master buoy deployed close to the mother ship and the others at intervals along the transect.

Depending on ice cover, the buoys will drift with the sea ice or the ocean for the duration of the mission. The AUV will be programmed to follow a path relative to the buoy positions, and the buoy positions will be transmitted via underwater acoustic communication to the AUV. The buoy positions must be updated, and thus, the AUV must be in communication range of at least one acoustic modem. We also want to space the buoys as far apart as possible to ensure an optimal range, while still ensuring the safety of the vehicle. An ice model is developed to predict the position of the navigation buoys, both to be able to predict buoy motion and to increase robustness in the event of extended communication loss.

This work was funded by the Research Council of Norway (RCN) through the Nansen Legacy Program, RCN #27272, and the Center of Excellence Autonomous Marine Operations and Systems (AMOS), RCN #223254.
*Corresponding author email: tore.mo-bjorkelund@ntnu.no

II. Related work

A. Ice drift forecasting

In [8], sea ice drift in summer was analysed and simulated with a temporal resolution of 12 hours. The work explored the interaction between wind, current and ice forces, and how they balance. Many sea ice models have coarse spatiotemporal resolution, multi-year, pan-arctic models [9], with the term *high resolution* used for models with $10km$ resolution [10]. Ensemble forecasting was used in [11] to assess the accuracy of an ice drift model. The method is widely used for forecasting as in [12], [13], and can give insight into the accuracy of a model.

B. Under ice operations

The first documented under ice operation with an AUV was conducted in 1972 [14]. AUVs have been used for increasingly complex tasks in the Arctic and under the ice, such as the pioneering cable laying operations performed by the Theseus AUV near Ellesmere Island in Canada [15]. The Theseus AUV, developed by the International Submarine Engineering Research Ltd. (ISE) laid 200 km of fiber optical cable under the ice, operating completely autonomously with a navigational error less than 0.5% of distance travelled. Acoustic positioning systems were placed both at the deployment site, as well as at the end of the transect at Ice Camp Knossos. In addition, one acoustic positioning system was placed approximately in the middle of the transect, allowing the vehicle to correct its

position underway. An experiment into the viability of ice-moored buoys with acoustic transponders was carried out by WHOI and the Office of Naval Research (ONR) in 2014, as presented in [16]. One of the challenges with under-ice navigation is that, unlike in the Theseus operation presented above, the AUV will often be above bottom-track range. This means that the AUV will not be able to measure the ground-relative velocity using the DVL. Moreover, due to sea-ice drift, the AUV navigation system may have to handle a moving target. Such was the case for the operation with the ISE Explorer AUV deployed off Boden Island in Canada [17], where the AUV was launched from a base to a remote camp on a drifting ice-floe ∼300 km offshore. The AUV transit towards the remote camp took 3 days, which meant that the acoustic homing system that was deployed at the remote site had to handle a possible 30 km drift. During 12 days under the ice without recovery, the ISE Explorer AUV collected close to 1000 km of sonar data. They reported that navigational drift was considerable in periods without DVL bottom-track or acoustic updates, but the AUV was consistently able to return to the remote camp for charging and data download due to the acoustic homing system.

III. Method

Our method has two main components, the first is the simulated ice drift, presented in Section III-A. The second component consists of estimates for velocity and direction of drift for each of the navigation buoys, as well as an estimate of the underlying velocity field, as presented in Section III-B.

A. Ice drift model

1) Vector field: The model consists of a vector field generated from a sum of time varying functions, such as the mean field, presented in (1), where $\boldsymbol{u}_0$ is the velocity vector, $\bar{u}$ is the mean velocity, and θ is the mean direction. $\epsilon_{\bar{u}}$, ϵ_θ are noise variables for the mean velocity and direction, respectively. Further, we introduce vorticity in (4), where $\boldsymbol{x}$ is the position in the vector field, $\boldsymbol{C_m}$ is the magnitude of rotation, and O_c is the origin of rotation generated from $\boldsymbol{O_c} \sim \mathcal{N}(\mu_o, \sigma_c^2)$ where we can with the desired accuracy place the origin. In order to represent the nugget effect [18], we add Gaussian noise to $\boldsymbol{u_2}$ in (7) where $\boldsymbol{U}$ is the tensor of vectors in the area and $\boldsymbol{\epsilon_j} \sim \mathcal{N}(0, \sigma_n^2)$ with σ_n^2 as the nugget effect variance. This variance is dependent on the spatial resolution of the model.

$$\boldsymbol{u_0} = \bar{u}[cos(\theta) \quad sin(\theta)]^\top \tag{1}$$

$$\dot{\bar{u}} = \epsilon_{\bar{u}} \tag{2}$$

$$\dot{\theta} = \epsilon_\theta \tag{3}$$

$$\boldsymbol{u_1(x)} = \boldsymbol{C_m}\frac{\boldsymbol{x} - \boldsymbol{O_c}}{||\boldsymbol{x}||} \tag{4}$$

$$\dot{\boldsymbol{O}}_{\boldsymbol{c}} = \boldsymbol{U(O_c)} + \boldsymbol{\epsilon_o} \tag{5}$$

$$\dot{\boldsymbol{C}}_{\boldsymbol{m}} = \boldsymbol{\epsilon_{C_m}} \tag{6}$$

$$\boldsymbol{U} = \Sigma_{i=0}^{N}\Sigma_{j=0}^{M}\boldsymbol{u}_i(\boldsymbol{x}_j) + \boldsymbol{\epsilon_j} \tag{7}$$

2) Nonlinear events: Nonlinear events (NE) such as pressure ridge formation and ice floe breakup are dependent on the divergence of the velocity field and cover of the ice. We model these nonlinear events as a Poisson distributed process where their probability is dependent on the divergence of the vector field and the ice cover. Thus, the probability of a nonlinear event at time t_n can be described as:

$$Pr(NE, t_n) = \frac{\lambda^k e^{-\lambda}}{k!} \tag{8}$$

where we can simplify to $k = 1$ and then only be dependent on λ. We chose

$$\lambda(T_i, \nabla \boldsymbol{V}) \propto \nabla \boldsymbol{V}, \frac{1}{T_i} \tag{9}$$

where T_i the ice thickness, and $\nabla \boldsymbol{V}$ is the divergence of the vector field. Ice thickness will be measured before the mission, while the divergence will be estimated from the buoy motion. The type of nonlinear event is determined by the sign of $\nabla \boldsymbol{V}$, where a positive divergence indicates lead formation, and negative divergence indicate pressure ridge formation. In the simulation, divergent ice flow can be simulated by having two models run simultaneously choose which one we sample based on location in the vector field.

3) Buoy motion: Buoy motion is simulated by choosing points in the vector field as the start position for the buoys and letting them propagate along the vector field. After the update of the buoy position, $\boldsymbol{U}$ is updated, and the process starts over until the desired time window has been simulated. We assume that the buoys are tethered to the ice or in case of a free floating buoy, the ocean (i.e. the buoy drift is equal to the ocean currents).

B. Modeling the vector field from buoy motion

In order to estimate the underlying flow field that is carrying the buoys, we first estimate the buoy drift.

1) Buoy drift model: As the buoys drift with the ice, they drift with a certain speed and direction, which are possible to estimate based on their position updates as:

$$\hat{v}_t = \frac{||\boldsymbol{p}_t - \boldsymbol{p}_{t-1}||}{\Delta t} \tag{10}$$

$$\hat{\theta}_t = atan2(\boldsymbol{p}_t - \boldsymbol{p}_{t-1}) \tag{11}$$

Where $\hat{v}_t$ is the speed estimate at time t, $\boldsymbol{p}_t$ is the position measurement at time t, Δt is the time difference between times t and $t-1$, and $\hat{\theta}_t$ is the estimated drift direction at time t. We model the speed and direction of travel as independent variables:

$$v_{t+1} = v_t + \beta_{v,t} + \epsilon_v \tag{12}$$

$$\theta_{t+1} = \theta_t + \beta_{\theta,t} + \epsilon_\theta \tag{13}$$

Where v_t is the speed at time t, θ_t is the direction of travel at time t, β is the rate of change, and ϵ is noise. We regard model uncertainty, measurement noise, and unmodelled ice

drift patterns as noise. In this model, we also assume that β can be modeled as a scalar value. We now define $\boldsymbol{x}_t = [v_t, \theta_t]^\top$ and $\boldsymbol{\beta}_t = [\beta_{v,t}, \beta_{\theta,t}]^\top$ In order to estimate $\boldsymbol{\beta}_t$, we seek to minimise the influence of ϵ by using a discrete time low-pass filter on $\hat{x}$:

$$\hat{\boldsymbol{x}}_t = \boldsymbol{\gamma}\hat{\boldsymbol{x}}_t + (1-\boldsymbol{\gamma})\hat{\boldsymbol{x}}_{t-1} \tag{14}$$

where $\boldsymbol{\gamma} \in [0, 1]$. Since the ice drift is a slow moving and slowly changing process in relation to the sampling rate, we can afford to set $\boldsymbol{\gamma}$ quite low. With most of the noise filtered, we can estimate the rate of change in speed and direction at time t; $\boldsymbol{\beta}_t$:

$$\hat{\boldsymbol{\beta}}_t = \frac{\hat{\boldsymbol{x}}_t - \hat{\boldsymbol{x}}_{t-1}}{\Delta t} \tag{15}$$

Rearranging (15), and propagating forward in time, gives us our estimate for the future buoy position:

$$\hat{\boldsymbol{x}}_{t+1} = \hat{\boldsymbol{x}}_t + \hat{\boldsymbol{\beta}}_t \Delta t \tag{16}$$

We do not take neighbouring buoys drift into account, since we are using (16) to predict the underlying vector field, as presented in the next section.

C. Vector field model

As the buoys are deployed in the ice, simulated or real, we continuously monitor their positions and estimate the underlying ice drift for the area. This is accomplished by Gaussian Process (GP) modeling [19] of the vector field of the ice in the operational area. We define the GP as:

$$f(\boldsymbol{x}) \sim \mathcal{GP}(m(\boldsymbol{x}), k(\boldsymbol{x}, \boldsymbol{x'})) \tag{17}$$

With mean function $m(\boldsymbol{x})$ and covariance function $k(\boldsymbol{x}, \boldsymbol{x'})$, where $\boldsymbol{x}$ is a vector estimated buoy drift directions and speeds. We use the radial basis function as a kernel for the GP. We assume that the buoys are fixed to the ice frame, as in [6]. The model of each buoy propagates forward in time to estimate their future positions and from this we estimate the AUV path length and end point location, as well as the future vector field.

D. Ensemble model propagation

In order to account for the relative simplicity of the buoy drift model, we draw an ensemble, $\boldsymbol{X}_{\boldsymbol{t}}^e$, of possible values for $\boldsymbol{x}$ and $\boldsymbol{\beta}$ at time t, where we assume that they are Gaussian, as presented in (18).

$$\boldsymbol{X}_t^e \sim \mathcal{N}([\hat{\boldsymbol{x}}_{\boldsymbol{t}}, \hat{\boldsymbol{\beta}}_{\boldsymbol{t}}]^\top, [\hat{\boldsymbol{\Sigma}}_{\boldsymbol{x}}, \hat{\boldsymbol{\Sigma}}_{\boldsymbol{\beta}}]^\top) \tag{18}$$

Where $\hat{\boldsymbol{\Sigma}}_{\boldsymbol{x}}$ is estimated by

$$\hat{\boldsymbol{\Sigma}}_{\boldsymbol{x}} = \frac{1}{N-1}\sum_{i=0}^{N}(\boldsymbol{x}_i - \hat{\boldsymbol{x}}_i)^2 \tag{19}$$

and $\hat{\boldsymbol{\Sigma}}_{\boldsymbol{\beta}}$ is estimated by

$$\hat{\boldsymbol{\Sigma}}_{\boldsymbol{\beta}} = \frac{1}{N-1}\sum_{i=0}^{N}(\boldsymbol{\beta}_i - \bar{\boldsymbol{\beta}})^2. \tag{20}$$

The ensemble is then propagated forward in time, using (16) for each time step. From these predictions, we can estimate the total path length and the location of the end point of the mission.

1) Path prediction: We know the buoy-relative plan for the AUV, and we know the desired speed of the vehicle. This enables us to iterate through (16) for all values in the ensemble, $\boldsymbol{X}_t^e$, while predicting the AUV path until the AUV reaches the end point. Enabling us to predict the position of the endpoint of the mission.

2) Scenarios for investigation: Modelling enables us to better understand the sensitivities of the overall system and simulate the AUV behavior in a range of different scenarios. We define three scenarios for investigation; all the buoys on one consolidated ice floe, a divergent scenario, and a dynamic situation with several floes. The instances are then generated randomly around the respective mean of the scenario and simulated to generate an ensemble of possible drift patterns. One instance of each scenario is presented in Figure 1.

E. Buoy drift prediction

The drift of the buoys are predicted using the method described above, estimating the direction and magnitude of the buoy drift. The velocity field is estimated by using the buoy drift data, using a GP. The magnitude and direction of the drift are assumed to be independent variables. From the forecasted ice drift, we can calculate the change in the AUVs path, as the AUV is programmed to follow a buoy-relative mission. The two main factors we are interested in are the relative increase in path length and the location of the end point of the mission at the end of the mission.

1) Pre mission modeling: We can start collecting data once the buoys are deployed, this will give the model a chance to estimate the average vector field, and thus the increase in the relative path length and the movement of the launch/recovery site.

2) Relative AUV path length: Once we are confident that the conditions are favorable for a mission, the AUV will be deployed and the mission will start. We define the relative AUV path length as the as the path length in the ice-fixed coordinate system measured in the earth-fixed coordinate system. The increase in path length is estimated by integrating the buoy-relative planned path over the mission, using past and forecasted buoy drift.

IV. Results

A. Increased path length

Over all the simulations we ran, we computed the theoretical path length of the AUV if it were to traverse from one starting buoy, to the final buoy and back. The buoys are simulated as to be deployed in a row as in Figure 1. The relative increase in path length is presented in Figure 2, where we see an increase in path length over 20% in some instances. There is an underlying assumption that the AUV travels at a set velocity of $1.5m/s$ in relation to the earth fixed coordinate system.

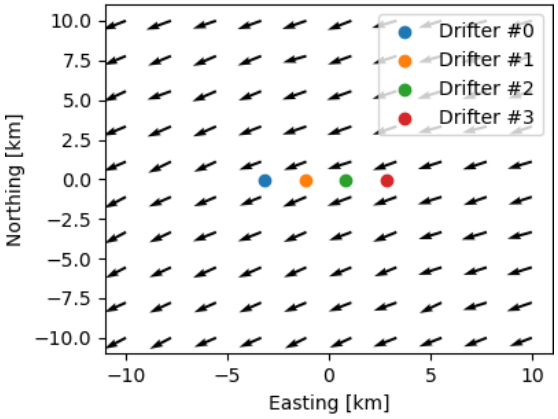

(a) Consolidated ice floe, high correlation in drift pattern of buoys.

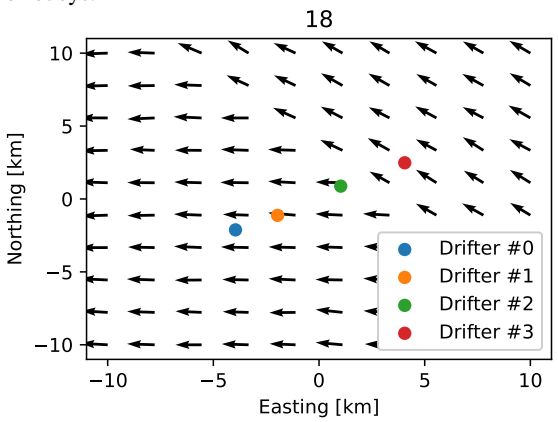

(b) Divergence in a lead formation scenario, multiple floes.

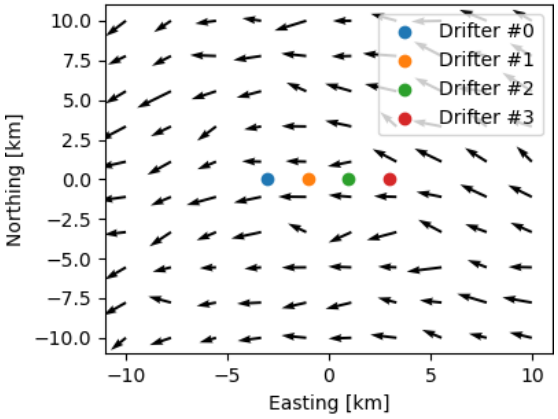

(c) Marginal ice zone scenario with less spatial correlation of drift direction and magnitude.

Fig. 1: Snapshots of three instances of simulated scenarios of the vector field and buoy locations.

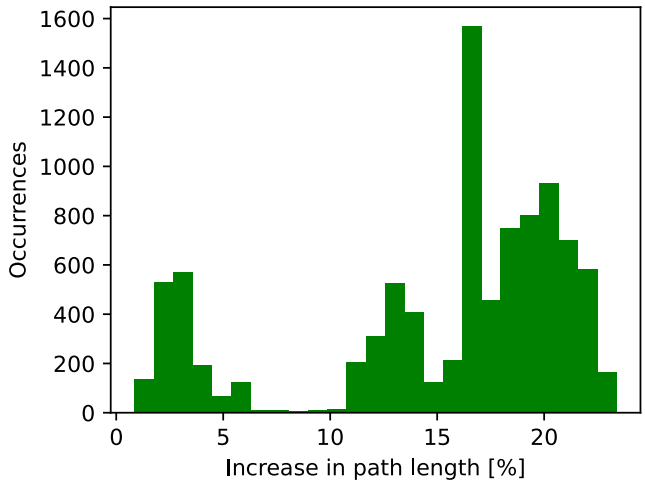

Fig. 2: Histogram of percent-wise increase in path length over several simulation scenarios.

B. Scenarios for investigation

We define three scenarios for investigation as presented in Figure 1.

- Consolidated drift ice
- Divergent drift ice - lead formation
- Marginal ice zone drift

We present the results from each of the simulated scenarios, with focus on forecasting accuracy. In addition, we present the divergence estimate in the divergent drift scenario and compare it with the divergence in the simulated vector field. In all scenarios we start with the buoys in the same positions, and with the same AUV mission; starting at the position of the first buoy, traverse all the buoys in order and come back to the starting buoy. We assume a vehicle surge velocity towards the target buoy of $1.5m/s$ in relation to the earth-fixed coordinate system. At each time step we simulate and forecast the Ensemble Endpoint Prediction (EEP). An instance of the consolidated drift scenario is presented in Figure 3. Additionally, we simulate the three scenarios with the same mean drift velocity, $0.25m/s$, and the same time step $\Delta t = 30s$, for better comparison.

C. Buoy drift Prediction

1) Consolidated ice floe: When simulating a consolidated ice floe, we increase the spatial correlation in the vector field in order to generate the most homogeneous buoy drift pattern of the three scenarios. The estimated variance and the mean error of the forecast is presented in Figure 4. We see that the forecast error is less than $1km$ for the entire mission, and that both error and variance are decreasing during the mission.

2) Marginal ice zone: When simulating the marginal ice zone, we decrease the spatial correlation in the vector field, otherwise we keep it equal to the consolidated ice floe scenario. The estimated variance and the mean error of the forecast is presented in Figure 4. In this case, the forecast error is above $1km$ at the start of the mission, but follows

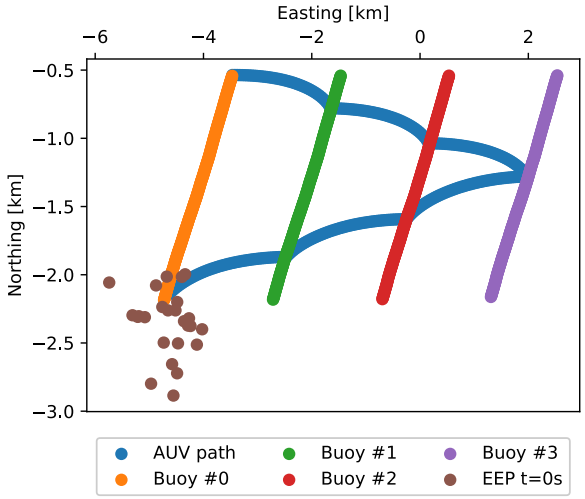

Fig. 3: Drift paths of the simulated buoys along with the simulated AUV path and the Ensemble Endpoint Predictions (EEP) for a consolidated ice drift scenario at the start of the AUV mission, $t = 0s$.

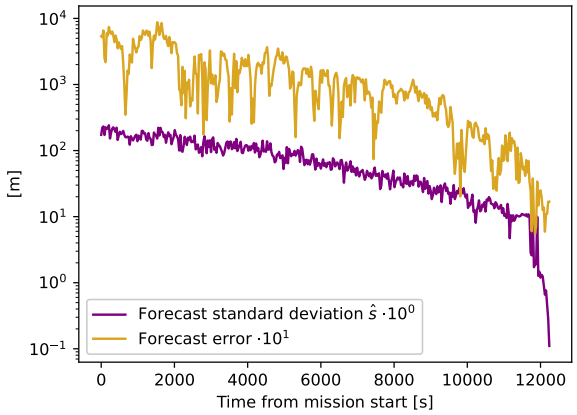

Fig. 4: Estimated standard deviation and mean error of the ensemble forecast of the endpoint of the mission for the consolidated ice floe scenario. Plotted with one decade separation.

the same trend as the previous scenario. We also see that the mission lasted longer than in the previous scenario.

3) Divergent ice flow: The divergent ice flow scenario is simulated by two independent, but similar simulation instances of the consolidated ice floe scenario, with a sharp separating boundary. This leads to some of the buoys having a higher correlation in motion than others. The forecast error and variance are the highest for this scenario, as shown in Figure 6, with a forecast error over $3km$. This mission was also the longest of the three scenarios, running for over $14000s$. For this scenario, we also present the GP of the vector field and the divergence of the field as seen in Figure 7. We see that the divergence is high around $[Northing, Easting] = [-5km, -10km]$, indicating

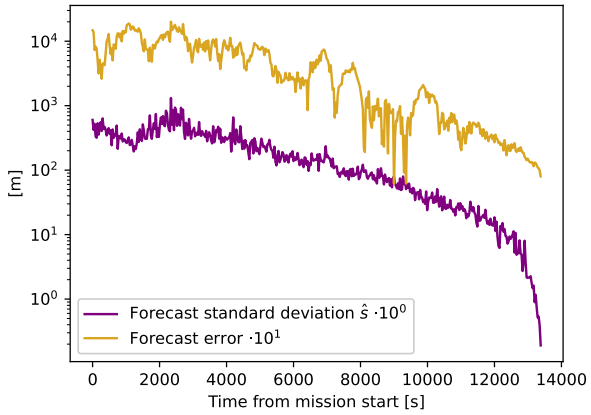

Fig. 5: Estimated standard deviation and mean error of the ensemble forecast of the endpoint of the mission for the marginal ice zone scenario. Plotted with one decade separation.

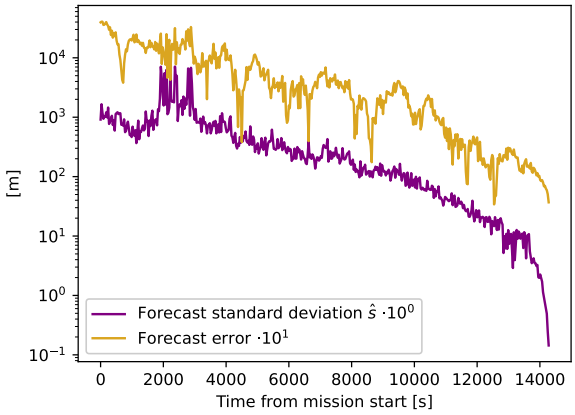

Fig. 6: Estimated standard deviation and mean error of the ensemble forecast of the endpoint of the mission for the divergent ice flow scenario. Plotted with one decade separation.

increased probability of lead formation in that area. In addition, there is negative divergence in the center of the area in the figure, indicating increased probability of pressure ridge formation.

V. Discussion

A. The AUV path

In this paper we have estimated the AUV path as a path going at each timestep directly towards the next target buoy without regard for currents, its depth or the lack of bottom-track in the Arctic. This means that the estimate for the increased path length due due buoy movement may be a lower bound, and thus having a bias towards being too liberal. The AUV path might also be extended by loss of communication with one or more buoy leading to a wrong course while the communication loss persists.

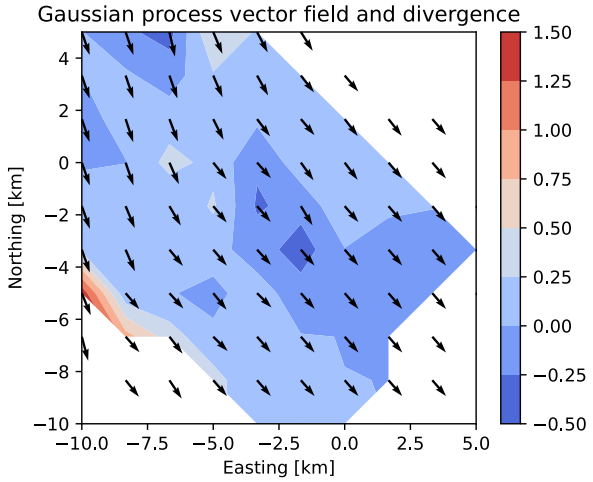

Fig. 7: Estimated standard vector field and divergence of the field from the Gaussian process.

B. Estimated end-point

In the ensemble forecast, $\hat{\beta}_t$, the rate of change of the velocity is assumed to have a Gaussian distribution. By propagating this forward in time to future positions, the estimates of the future positions are not Gaussian, which might not be optimal. Comparing Figures 4, 5 and 6, it seems that model accuracy is dependent on correlation of motion in the buoys. This can be expected since the model relies on past trends propagating into the future.

C. Modelling a simulation

This paper has presented a method for both modelling and estimating ice drift from said model. Since we are modelling a simulation, we have no guarantee that the work will be relevant. We assert that the process has had value by planning to use the method presented in this paper in the preparation for and during the operation in May, using real data from buoys deployed in the ocean or in the ice.

VI. Conclusion

In conclusion, we are able to simulate a vector field driving buoy drift for testing and development of forecasting for ice drift. The ensemble forecast has shown the ability to predict future ice locations and underlying properties of the motion of the simulated ice. Further work includes adding input from ship based measurements such as wind and current measurements in addition to ice radar measurements. As the preparation for the under ice operation continues, the forecasting tool presented here will continue to evolve.

References

[1] G. Johnsen, M. Norli, M. Moline, I. Robbins, C. von Quillfeldt, K. Sørensen, F. Cottier, and J. Berge, "The advective origin of an under-ice spring bloom in the arctic ocean using multiple observational platforms," *Polar biology*, vol. 41, no. 6, pp. 1197–1216, 2018.

[2] A. Kukulya, A. Plueddemann, T. Austin, R. Stokey, M. Purcell, B. Allen, R. Littlefield, L. Freitag, P. Koski, E. Gallimore *et al.*, "Under-ice operations with a remus-100 auv in the arctic," in *2010 IEEE/OES Autonomous Underwater Vehicles*. IEEE, 2010, pp. 1–8.

[3] R. E. Francois and W. E. Nodland, "Unmanned Arctic research submersible system development and test report," University of Washington, Tech. Rep. No. APL-UW 7219, 1972.

[4] J. Strutt, "Report of the inquiry into the loss of Autosub2 under the Fimbulisen," National Oceanography Centre, Southampton, U.K., Tech. Rep. 12, 2006. [Online]. Available: http://eprints.soton.ac.uk/41098/

[5] P. Norgren, "Autonomous underwater vehicles in arctic marine operations: Arctic marine research and ice monitoring," Ph.D. dissertation, Norwegian University of Science and Technology (NTNU), 2018.

[6] P. Norgren, T. Bjørkelund, K. Gade, Ø. Hegrenæs, and M. Ludvigsen, "Intelligent Buoys for Aiding AUV Navigation Under the Ice," in *Proc. IEEE/OES AUV*, St. John's, NL, Canada, 2020, pp. 1–6.

[7] L. Freitag, M. Grund, S. Singh, J. Partan, P. Koski, and K. Ball, "The WHOI micro-modem: an acoustic communications and navigation system for multiple platforms," in *Proc. MTS/IEEE OCEANS*, Washington, DC, USA, 2013, pp. 1086–1092.

[8] M. G. McPhee, "An analysis of pack ice drift in summer," *Sea ice processes and models*, pp. 62–75, 1980.

[9] W. Hibler III, "A dynamic thermodynamic sea ice model," *Journal of physical oceanography*, vol. 9, no. 4, pp. 815–846, 1979.

[10] P. Rampal, S. Bouillon, E. Ólason, and M. Morlighem, "nextsim: a new lagrangian sea ice model," *The Cryosphere*, vol. 10, pp. 1055–1073, 2016.

[11] A. J. Schweiger and J. Zhang, "Accuracy of short-term sea ice drift forecasts using a coupled ice-ocean model," *Journal of Geophysical Research: Oceans*, vol. 120, no. 12, pp. 7827–7841, 2015.

[12] T. N. Krishnamurti, C. Kishtawal, Z. Zhang, T. LaRow, D. Bachiochi, E. Williford, S. Gadgil, and S. Surendran, "Multimodel ensemble forecasts for weather and seasonal climate," *Journal of Climate*, vol. 13, no. 23, pp. 4196–4216, 2000.

[13] P. Bauer, A. Thorpe, and G. Brunet, "The quiet revolution of numerical weather prediction," *Nature*, vol. 525, no. 7567, pp. 47–55, 2015.

[14] R. E. Francois and W. E. Nodland, "Unmanned Arctic research submersible system development and test report," University of Washington, Tech. Rep. No. APL-UW 7219, 1972.

[15] J. Ferguson, A. Pope, B. Butler, and R. Verrall, "Theseus AUV – two record breaking missions," *Sea Technology*, vol. 40, no. 2, pp. 65–70, 1999.

[16] L. Freitag, K. Ball, J. Partan, P. Koski, and S. Singh, "Long range acoustic communications and navigation in the arctic," in *OCEANS 2015-MTS/IEEE Washington*. IEEE, 2015, pp. 1–5.

[17] C. Kaminski, T. Crees, J. Ferguson, A. Forrest, J. Williams, D. Hopkin, and G. Heard, "12 days under ice - an historic AUV deployment in the Canadian High Arctic," in *Proc. IEEE/OES AUV*, Monterey, CA, USA, 2010, pp. 1–11.

[18] N. Cressie and C. K. Wikle, *Statistics for spatio-temporal data*. John Wiley & Sons, 2015.

[19] C. E. Rasmussen, "Gaussian processes in machine learning," in *Summer School on Machine Learning*. Springer, 2003, pp. 63–71.